Design and Beam Dynamics Study of the Magnet System for an 11 MeV Superconducting Isochronous Cyclotron

PanPan Zheng,[1,2] XiangHui Wang,[3] ZiFeng He,[2] Yue Wu,[2] ZhiMin Dai,[2] and Weishi Wan[1,*]

[1]*School of Physical Science and Technology, ShanghaiTech University, Shanghai 201210, China*
[2]*Shanghai Institute of Applied Physics, Chinese Academy of Sciences, Shanghai 201800, China*
[3]*School of Computer Engineering, Weifang University, Weifang 261061, China*

In recent years, due to the scarcity of radioisotopes domestically, the Chinese government has strongly supported the development of dedicated radioisotope production facilities. This paper presents the conceptual design simulations of an 11 MeV, 50μA, H^- compact superconducting cyclotron for producing radioisotopes. This paper primarily focuses on four aspects: magnet system design, central region configuration, beam dynamics analysis, and the extraction system design. The paper outlines the cyclotron's primary parameters and the key steps in the development process.

Keywords: superconducting cyclotron magnet, beam dynamics, central region, stripping extraction

I. INTRODUCTION

Medical isotope production is an important area of the field of nuclear medicine and medical imaging[1, 2]. These isotopes are widely used in the diagnosis and treatment of various diseases, especially in cancer treatment and heart disease diagnosis. Many medical isotope are produced in cyclotrons by bombarding the target with protons or other particles. Cyclotrons play a vital role in the production of medical isotopes[3–5], offering an efficient and flexible method to meet the demands of modern medical diagnosis and treatment. Due to the shortage of radioisotopes in the present world, the medical isotope production and supply systems are being actively developed[6–8]. As is widely recognized, low-energy cyclotrons are primarily employed for proton therapy[9–11], radioactive isotope production, etc[12, 13]. Most existing cyclotrons use normal conducting magnet systems, with the maximum field of approximately 2 T. Employing superconducting technology can easily elevate the average field of a cyclotron to approximately 4-5 T and even 9 T in some cases[14]. Therefore the smaller magnet radius can yield higher energy, resulting in a decrease in its size and overall mass (roughly proportional to $\frac{1}{B^3}$). Furthermore, a notable advantage of employing high magnetic fields in low-energy cyclotrons is that the entire magnet (including yoke) can be accommodated within a compact cryostat. In addition, the superconducting technology has the advantages of increasing the stability of the magnetic field, reducing maintenance costs, lowering energy consumption, saving operating costs and extending operating time, etc. Hence, there is considerable enthusiasm for the design of superconducting cyclotrons[15]. This paper primary focuses on designing a magnet system that accelerates H^- to an extraction energy of E_k=11 MeV, using a superconducting cyclotron magnet system for isotope production. In comparison to existing cyclotrons, this design features a more compact structure achieved, through the use of spiral magnets, a more convenient adjustment of the isochronous field by adding magnets of specific sizes in the valley and a simpler extraction system using stripping extraction. Furthermore, a phase selector has been added in the central region to avoid the potential damage caused by particles loss in other areas, which makes it easier to maintain the device.

This cyclotron utilizes an internal source structure, which is a Penning Ionization Gauge(PIG)[16] source, located near the center of the cyclotron. Owing to the low flutter in the central region, the magnetic field is unable to supply adequate axial focusing for the beam. Consequently, the primary deficiency in axial focusing from magnetic field occurs in the central region. The central region needs to be well-designed to obtain sufficient electrical focusing to obtain sufficient beam capture acceleration, and beam centering is crucial for achieving high final beam quality. So a well thought-out central electrode design is crucial to ensure sufficient electric focusing for the beam, which accounts for the complexity inherent in the design of the central region. The extraction system employs a stripping device to extract the proton beam, which subsequently produces the required medical isotopes by bombarding an external target. Furthermore, the conversion of H^- ions into protons through stripping is utilized to augment beam extraction efficiency, potentially reaching near 90%[17]. Using an external target can help keep the extraction region clean and the size of the stripping device is not limited by the hill gap. The design of the main magnet must not only ensures the stable acceleration of the beam but also provides sufficient space for installing the ion source and the stripping device. This makes it an iterative process and a critical phase in cyclotron development. The preliminary layout of this magnet system is determined in accordance with magnetic circuit law. Simulation of the magnetic field is obtained through modeling and finite element analysis utilizing OPERA/TOSCA[18]. To achieve steady acceleration of the beam, two conditions need to be fulfilled, which are that the magnetic field satisfies the isochronous criterion and provides sufficient axial focusing for the beam. Achieving field isochronism is of paramount importance, which can be accomplished by fine-tuning the sector angular width, sector spirality, and the hill and valley gaps. Accurate calculation of beam dynamics is essential to obtain precisely both the isochronicity of the field and the motion characteristics of

* Corresponding author, wanwsh@shanghaitech.edu.cn

the beam. The DONS[19] and OPAL[20] programs[21] are used for particle tracking in the 3D electromagnetic fields. OPAL is a tool from PSI that can be used for cyclotron design, DONS is a cyclotron design code developed at University of Science and Technology of Chain by Dr.Xianghui Wang.

In this paper, static equilibrium orbit analysis and beam tracking are performed. The structure of the central region and the angle of Dee are optimized by multi-particle simulation results. The evaluation of the field isochronicity is achieved by observing the phase offset of a single particle during the acceleration process. The effect of beam matching on the beam radial emittance is studied through beam dynamics simulation. The final beam radial emittance are minimized by carefully matching the initial phase space ellipse of the beam to the optimal one downstream and the judicious selection of the RF phase. which results in obtaining optimal characteristics of the final beam, namely, efficiency and emittance. The appropriate stripping point is chosen by observing the variation of the beam envelope during the acceleration process. Subsequently, the position and dimensions of the stripping foil are refined by analyzing how its azimuthal position and tilt angle relative to the beam affect the extraction of the beam. This arrangement enables extraction by utilizing the stripping foil's dual opposite positions to guide the beam more effectively[22]. Based on these design considerations, we present a main magnet system for a low-energy, compact superconducting cyclotron for the stable acceleration of H^- ions. Due to the compact, flexible, and convenient design advantages, this cyclotron is planned for use in the production of medical radioisotopes.

II. MAGNET DESIGN

In order to solve the problem of obtaining the total energy within the confines of a magnetic constraint due to relativistic mass increase by the factor (1). Thomas proposed the innovative concept of the isochronous cyclotron. The isochronous field is scaled by the relativistic factor γ with respect to radius ($B = \gamma \cdot B_0$)[23]. The phase stability of ions is obtained through its azimuthally-symmetric isochronous design, while the axial (vertical) stability of ions is achieved through the introduction of azimuthally-varying-field (AVF). But, in case of high magnetic field in a superconducting cyclotron, magnetic field flutter of the Thomas-type cyclotron is too small to provide sufficient traverse focusing. As a result, spiral sectors were adopted to increase the edge angle and the number of sectors were reduced to increase flutter. Based on these considerations, the magnet system of the 11 MeV cyclotron employs a three-fold symmetric, compact, spiral magnetic structure, which plays a pivotal role in facilitating axial focusing for ions at large radii.

$$\gamma = \frac{E}{(m_0 c^2)} \tag{1}$$

$$B(r) = \frac{m_0 c}{qr} P \cdot (1 - \frac{\delta_2}{P^2}) \tag{2}$$

$$B(0) = \frac{2\pi f m_0}{q} \tag{3}$$

$$\rho = \frac{\sqrt{E_k \cdot (E_k + 2E_0)}}{Bqec} \tag{4}$$

The main parameters can be roughly estimated using simple analytical calculations[24, 25]. An effective magnet design must satisfy the following three essential criteria:

(1) The magnetic field must increases with the radius to maintain the isochronous condition throughout the acceleration process.

(2) Azimuthally-varying-field focusing is achieved by configuring the magnet pole into a set of three Archimedean spiral sectors while maintaining a consistent average magnetic field. Each angular width of 60^o. There is sufficient axial and radial focusing for the beam to obtain optimal transverse beam envelope during acceleration.

(3) The radial and axial betatron tunes must be sufficiently far from dangerous resonances or pass through resonance bands rapidly to ensure stable operation.

To obtain the ideal isochronous field, the Gordon method[26] is employed for calculation, the magnetic field must satisfy the following formula (2), the value of the magnetic field at the center for a given angular frequency can be obtained using formula (3) with r=0. Upon determining the extraction energy and the value of the magnetic field at the center, the preliminary estimation of the extraction radius can be calculated using equation (4), where E_k is the kinetic energy of the particle and E_0 denotes the rest energy of the particle. The intensity of the magnetic field at the center is found to be 3.03 T. Due to the H^- lifetime issues caused by magnetic stripping, it is safe to select a conservative value of 3 T for the magnetic field at the center without loss of the H^- beam[27]. This value of the central field is significantly lower than the 4.5 T central field of the existing small cyclotron ION-12SC, making it suitable for stripping extraction. The ion's angular frequency is calculated as $f = 15.36 \cdot B_0$, yielding a value of 46 MHz. This RF frequency is lower than that of existing cyclotrons, such as the 68 MHz RF frequency of the ION-12SC, making it easier to achieve in both manufacturing and operation. Based on the equations (5) and (6), it can be preliminarily estimated that the magnetic field intensity in the extraction region is approximately 3.07 T, and the beam extraction radius is about 160 mm.

$$B_f = B_0 \cdot (1 + \frac{E_k}{E_0}) \tag{5}$$

$$r_f = \frac{E_0}{300 B_f} \cdot \sqrt{(\frac{B_f}{B_0} - 1)^2 + 2(\frac{B_f}{B_0} - 1)} \tag{6}$$

$$R = \frac{r_f}{\zeta} \tag{7}$$

It can be concluded from eq.(7) that the magnet's radius falls within the range of 173 mm to 200 mm. Here, ζ represents the correction coefficient for the magnet, whose value ranges from 0.78 to 0.91. To accommodate the installation of other components and provide sufficient room for the magnetic poles, the sector radius is selected to be 200 mm after further optimization. Furthermore, considering the relationship between the spiral angle and the radius of the magnetic pole, it becomes evident that the maximum spiral angle of the magnetic pole is 64^o. This angle is well within the capabilities of standard machining processes, making it a feasible choice for implementation. The cyclotron RF system adopts a 197^o single-dee configuration and operates in the 1st harmonic acceleration mode. The rationale for selecting this model will be discussed in the following section. The hill gap of 30 mm is chosen to leave an installation location to accommodate the RF system. The cross-section of coil is $55\,\mathrm{mm} \times 45\,\mathrm{mm}$, with a total ampere-turns of 420000 A. The coil's current density is selected to be $170\,\mathrm{A/mm^2}$[28]. In summary, the fundamental parameters of the cyclotron are shown in Table 1.

Table 1. Basic parameters of the cyclotron

Item	
Cyclotron type	Compact, Isochronous
Accelerated particle	H^-
Final energy / Current	11 MeV, 50μA
Central / extraction field	3.032 T / 3.067 T
Sectors / Sector shim type	3 / Archimedean spiral
Spiral angle(maximum)	64^o
RF system	One 197^0 Dee, 30 kV
Injection type	Internal PIG source
Operation RF harmonic	1
RF frequency	46 MHz
Extraction radius	160 mm
Hill gap	30 mm
Operating current density	170 A/mm^2
Cyclotron high	730 mm

Based on the magnet parameters presented in Table 1, the $1/3$ model is created by SOLIDWORKS and subsequently imported into OPERA/TOSCA for simulation calculation. The simulation model is visually represented in Fig.1(a). After a series of simulation iterations, the mean field is adjusted to match the isochronous field at the median plane using the Gordon method. Fig.1(b) gives a comprehensive representation of the median-plane mean field that satisfies isochronicity. The central field B_0 is 3.032 T, the minimum field is 2.365 T, and the maximum field reaches 3.643 T. Various techniques[29] can be employed to approach the ideal isochronous field, such as modifying the sector angular width, adjusting the spiral angle, and refining the hill gap and valley gap, etc. The sector angular width and spiral angle remain unchanged throughout the optimization process. Since the RF system is not installed in the valley, the magnetic field is adjusted by modifying the valley gap at different radii. This goal can be achieved by adding magnets of specified sizes at different radii in the valley. Due to the compact size of the cyclotron, the advantage of doing so is that it is easy to implement in practice. In addition, if necessary, it is convenient to accelerate other particles by adjusting the size of the added magnets according to the isochronous field requirements. This method has lower precision requirements for coil positioning compared to adjusting the superconducting coil, and it offers higher adjustability.

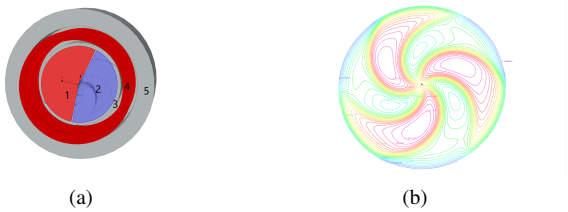

(a) (b)

Fig. 1. (a) 3D model of the upper half of the magnet in OPERA: 1-Dee, 2-dummy Dee, 3-magnet pole, 4-coil, 5-yoke; (b) density map satisfies isochronicity

Fig.2(a) presents both the ideal isochronous field obtained by the Gordon method and the distribution of the azimuthal mean field obtained by the model, plotted as a function of radius. It can be seen that the deviation between the simulated field and the ideal isochronous field remains within 10 G range throughout the acceleration region. In order to achieve weak focusing at the central region to satisfy the axial stability requirement of particles, the magnetic field in the range r=0-20 mm exceeds the theoretical isochronous field. The betatron frequencies is calculated from small perturbations of the equilibrium orbit. Fig.2(b) illustrates the variation of the orbital frequency error with energy and the orbital frequency error throughout the entire acceleration process maintaining a remarkable low level of within 0.02%. From this perspective, the isochronous field error staying within 10 G falls within the acceptable range of error. This error will be verified more precisely through beam dynamics simulation in subsequent stages. In addition to satisfying the isochronous condition, the magnetic field distribution must also deliver an ample transverse force to effectively focus the particle beam. The radial and vertical beam tunes are intricately linked to various parameters of the magnetic sectors, including the radial field index, spiral angle, field flutter, etc. The working point of the cyclotron is effectively away from the dangerous resonance state by fine-tuning the spiral angle of the magnetic pole. Fig.2(c) presents the static equilibrium orbit(SEO) ringing from 1 MeV to 11 MeV. It's evident that each orbit oscillates around a specific radius, and the concentric distribution of these orbits demonstrates effective isochronous field regulation. Fig.2(d) illustrates the working point diagram for the 11 MeV cyclotron design, calculated from magnetic field map produce by OPERA using OPAL and DONS. There is little difference between the calculations from the two codes. Notably, the diagram demonstrates that particles effectively avoid crossing any dangerous resonance lines(the dotted lines represent the different resonance lines) throughout the acceleration process.

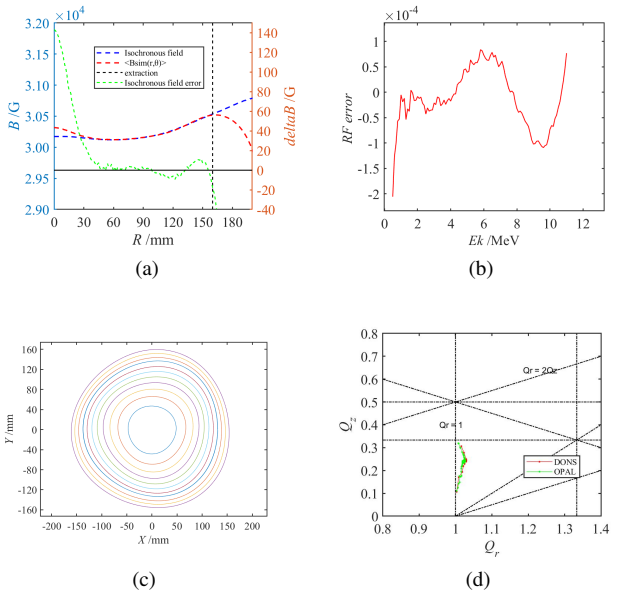

Fig. 2. (a) the designed magnetic field compared with the ideal isochronous field and the isochronous field error; (b) the variation of the orbital frequency error with energy; (c) the static equilibrium orbit from 1 MeV to 11 MeV; (d) Working point diagram

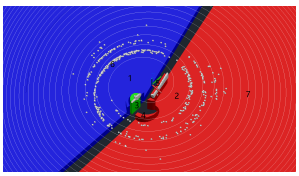

Fig. 3. Schematic diagram of RF model: 1-dummy Dee, 2-Dee, 3-ion source, 4-puller, 5-phase selector, 6-beam loss, 7-reference particle trajectories.

III. CENTRAL REGION

The design of the central region structure significantly affects the intensity and quality of the extracted beam[34**?** , 35]. In order to enhance the transmission efficiency in the central region and the quality of the extracted beam, the design of the central area should consider the following aspects:

(1) The central region structure should have a fixed phase acceptance. It is crucial to maximize the phase acceptance of the central region. This is crucial for enhancing the beam transport efficiency within central region.

(2) Reducing the beam phase dispersion and optimizing the beam centering in the first few turns play a decisive role in improving the quality of the extracted beam.

(3) The quality of the beam at the point of entering the extraction system is a critical factor influencing both the efficiency of extraction and the quality of the beam extracted.

The RF resonator, with a Dee radius of 180 mm, accommodates itself between the spiral pole faces. The Dee plates are 3 mm thick and spaced 10 mm apart. The structural model of the Dee and the central region are utilized to determine the electrical field distributions employed in the beam dynamics analysis. Fig.3 presents the model structure for the central region. An ion source of PIG type with an internal chimney radius is 2 mm is employed. The dimension of the ion source opening slit of $0.2 \times 2\,\mathrm{mm}^2$. The most commonly used shape of the source slit is one whose axial size is several times greater than its radial size[30]. The gap between the Dee and the dummy Dee is 6 mm, with the peak voltage set at 30 kV. Compared to the central region design of the ION-12SC, this design increases the gap between the dee and dummy dee, which enhances the dee voltage, improves acceleration efficiency, and reduces acceleration time.

In the case of the PIG-type ion source, where the initial beam energy is typically low, the time taken for particles to traverse the first acceleration gap is non-negligible. At the output silt of the ion source, the beam energy typically ranges between 5 eV and 20 eV, with an emittance of approximately 1.3π mm mrad[31]. When generating the initial particle distribution injected from an internal source, it is necessary to consider the dependence of the extracted beam intensity on the extraction voltage amplitude, which is described by the Child-Langmuir law[33]. Following Kirkpatrick's formula[32], ignition occurs when the value is higher than 1.3 Kirkpatrick in the experiment. (1 Kirkpatrick equals to 86kV/cm at 46 MHz.) After preliminary calculation, the width of the first acceleration gap should be approximately 3.5mm. The first acceleration gap significantly influences the particle trajectory and other beam dynamics characteristics, so the design of the first acceleration gap is the primary consideration in the central region design. In the central structure of the internal ion source, beam parameters can be adjusted by manipulating the position and direction of the ion source opening slit. Based on the centering of the beam and energy gain in the initial turns of the particle, the position of the ion source, the initial direction of the particle, and the starting RF phase at the output slit of the ion source are optimized. More details are presented in the next section. Following the optimization of the ion source's placement, that optimal beam centering is attained, that the ion source is positioned at (-0.2mm, -7mm), and the radius is 7.0029 mm.

It is necessary to analyze the acceleration process of particles with various initial phases since the central region exhibits different acceptance characteristics for particles injected at different times. First, from the perspective of the energy gain, Fig.4(a)(b) clearly illustrates the trajectory of particles with different initial phases in the first few turns and the energy gain through the first acceleration gap. It is evident that the energy gain of particles with an initial phase distribution of -90^o to -40^o and 0^o to 90^o is significantly smaller than that of particles with an initial phase distribution of -40^o to 0^o. Secondly, the analysis is conducted from the standpoint that particles are subject to focusing/defocusing. According to theoretical analysis, particles approaching the phase where the electric field is about to decrease experience a greater focusing effect as they pass through the center-line of the acceleration gap. Fig.4(a) reveals that axial defocusing acts on particles passing through the first acceleration gap when the initial phase distribution is between -90^o and -60^o, while

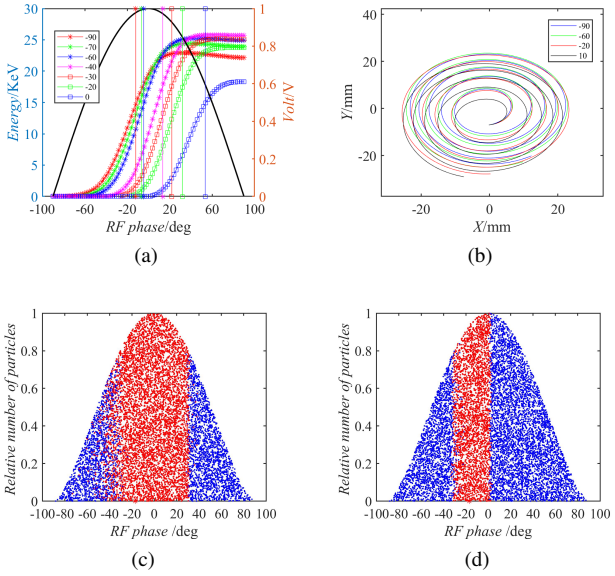

Fig. 4. (a) different initial phase .vs energy gain after crossing the first acceleration gap; (b) trajectory of particle; (c) phase acceptance for initial; (d) phase acceptance for optimal. blue dots-ions injected from ion source,red dots-ions accepted into acceleration

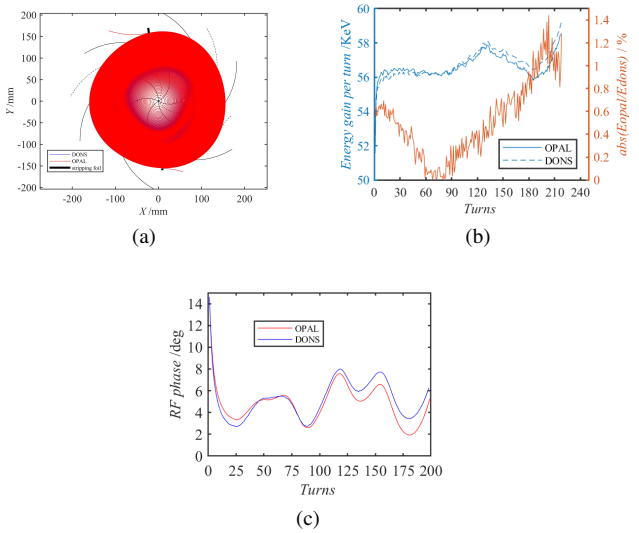

Fig. 5. (a) particle tracking; (b) energy gain per turn; (c) RF phase excursion.

axial focusing is applied to particles with a phase between -60^o and 0^o. The analysis above indicates that particles with initial phases ranging from -40^o to 0^o exhibit better energy gain and focusing effects.

It is necessary to design the central region to ensure that the beam undergoes sufficient axial focusing as it traverses the first few acceleration gaps. This is crucial due to the low initial energy at the output slit of the ion source, which defocuses the beam. The initial RF model utilizes a 180^o Dee structure, in which case the phase of the second pass through the accelerated gap midline is 170^o, when the particles experience axial defocusing for the first few turns resulting in the low transmission efficiency of 26.5%. Optimizing the Dee structure enhances transmission efficiency in the central region by providing axial focusing during the second acceleration gap in the initial turns. With the selection of the single 197^o Dee structure, the optimized central region transmission efficiency is 62%. Multi-particle simulation results show that particles within the range of 0^o to 30^o could traverse the central region but were not successfully extracted due to growing de-centering of the beam, as shown in Fig4(d). The results of the multi-particle simulation also indicate that the phase acceptance in the central region is -30^o to 30^o without the phase selector. Under this condition, the transmission efficiency for the first few turns is 62% with only 35% achieving acceleration to the full energy. A phase selector has been incorporated into the central region to selectively discard particles with initial phases ranging from 0^o to 30^o. This measure aims to reduce energy dispersion and radial oscillation amplitude in the extracted beam, consequently improving the overall quality of the extracted beam. Furthermore, particles with phases between 0^o and 30^o will be lost in other parts of the cyclotron, potentially causing damage. Therefore, it is better to add a phase selector in the central region to ensure that these particles are lost within the phase selector. Periodically changing the phase selector is more convenient and effective than dealing with the potential damage caused by particle loss in other areas. Finally, the transmission efficiency of particles in the first few turns is 40% with 30% capable of accelerating to full energy. The trajectory of beam particles captured in central region acceleration is illustrated in Fig.3.

IV. BEAM DYNAMICS CALCULATIONS

A. single-particle tracking

Field isochronism and tune optimization are critical considerations in the design process of the cyclotron magnet. Therefore, it is essential to conduct a thorough assessment of field isochronism and carefully examine both axial and radial beam focusing through single-particle tracking. The radial and axial betatron tunes of the particles are studied, and the working point diagram of the cyclotron based on the SEO is constructed in the previous section. Subsequently, a comprehensive exploration of the beam's properties during the acceleration phase will be studied. The phase offset within the accelerating region is obtained from the beam dynamics analysis to ensure that it meets the isochronous requirements(see Fig.5(c)). The acceleration voltage experienced by a particle as it traverses an acceleration gap is described by the equation $V = V_0 cos\phi$, where V_0 represents the maximum voltage of the RF system.

Results from single-particle tracking reveal that particles demonstrate enhanced beam centering characteristics and energy gain. The first turn energy gain is 53.3 KeV, corresponding to a radius of 10 mm. Consequently, the estimated dis-

tance of the ion source from the machine center is approximately 7 mm. The trajectory of a single particle is calculated using OPAL and DONS respectively. Fig.5(a) illustrates the trajectory of an H^- particle undergoing acceleration from 20 eV to 11 MeV (with the bunch position at roughly r=155 mm). The particle achieves 11 MeV after completing 191 turns of acceleration. This indicates the high effectiveness of the beam centering, as well as the consistency in tracking results between the two codes. Fig.5(b) represents the particle's energy gain per revolution, and the kinetic energy of H^- ion as a function of the turn number throughout the acceleration process. The computed energy gain per particle turn is approximately 57 KeV, with a negligible relative error of within 1.5% between the results obtained from the two programs. Fig.5(c) illustrates the RF phase of the H^- ion as it traverses the Dee gap. The mean field dependence on the number of turns exhibited a slight deviation from the isochronous curve. Consequently, this led to slippage in the RF phases of the particles. Fig.5(c) demonstrates that the total RF phase excursion during the acceleration process remains within 5^o, reflecting the high degree of isochronicity of the magnetic field. The similarity in trends of the phase excursion calculated by two codes further confirms the accuracy of the simulation results.

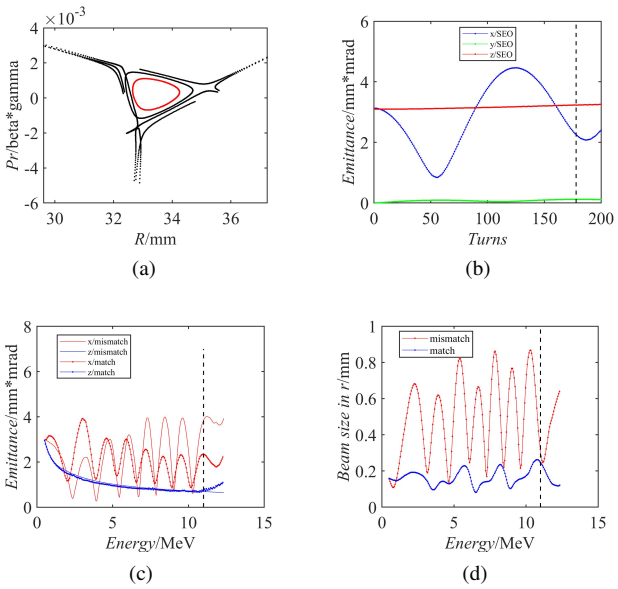

Fig. 6. (a) The radial phase space motion of the beam near the static equilibrium orbit; (b) Evolution of beam emittance with turn number; (c) Evolution of beam emittance with energy; (d) Evolution of beam size in radial with energy

B. Tracking of an ensemble of particles

Tracking of an ensemble of particles is necessary to investigate the impact of magnetic field on the beam focusing and transmission efficiency. Calculations are conducted using a bunch of 10,000 macro-particles. Observations show an increase in emittances(projections on phase-space planes) as the beam undergoes acceleration within the central region. The beam exits the ion source opening slit and accelerates to 0.5 MeV after 10 turns, the radial beam emittance is approximately 3π mm mrad. The results show that the radial emittance increases from 3π mm mrad to 10.15π mm mrad (at E_k=11 MeV) when a mismatched distribution is observed. This phenomenon results in degraded beam quality at extraction. To reduce this effect, the initial beam distribution are studied comprehensively to optimize the quality of the extracted beam.

Subsequently, the influence of the stable region of radial motion[36] on the emittance of the beam throughout the acceleration process is studied. The initial particle distribution from the ion source slit is assumed to be an uncoupled Gaussian distribution. The particle bunch evolves under the influence of the fields generated by the simplified azimuthally symmetric cyclotron. It will self-generate into a circular stationary distribution after the first several turns. The primary focus is on achieving radial matching. After obtaining the SEO of particle at 0.5 MeV energy, the deviations in the particle's position(r) and radial momentum(pr) from the SEO are adjusted, and these parameters are recorded after each turn. The radial phase space motion of the beam near the SEO is obtained by different phase space trajectories under different initial conditions, as shown in Fig.6(a). The red area indicates the stable region. The Twiss parameters of a beam with an emittance of 3π mm mrad in the stable region can be obtained easily.

To confirm the compatibility of this distribution, particles are tracked multiple turns within the cyclotron at 0.5 MeV beam energy without an RF system. As illustrated in Fig.6(b), the observed minor oscillation of the beam emittance can be attributed to the inherent non-linearity within the magnet system. The periodic nature of radial beam emittance oscillation without acceleration stems from the non-integer values of the radial betatron tunes Q_r, ranging between 1.004 and 1.027. Similarly, the marginal fluctuations observed in axial beam emittance are attributed to axial betatron tunes falling within the range of 0.0998 and 0.32. These findings align with theoretical expectations.

This paper provides a detailed study of beam emittance evolution during the acceleration process in two scenarios: a mismatched beam and a beam with particles distributed within radial stability. The simulation results depicted in Fig.6(c) indicate that the radial equilibrium matched beam exhibits significantly lower emittance than the unmatched beam throughout the acceleration process and the emittance of the matched beam decreases to 2.36π mm mrad at the extraction. Fig.6(d) shows the evolution of the radial envelope for all two scenarios during acceleration. It is evident that the mismatched beam experiences pronounced radial oscillations spanning from 0.1 mm to 1.2 mm, whereas the matched beam displays a considerably narrower range of variation in its radial envelope, fluctuating between 0.08 mm and 0.26 mm. This reduction in beam emittance and beam envelope enhances the quality of the extracted beam and extraction efficiency.

V. EXTRACTION SYSTEM

As widely recognized, cyclotrons used in radioisotope production typically have lower beam quality compared to those intended for fundamental research and cancer therapy. Consequently, this cyclotron design adopts the stripping extraction method commonly used in negative ion accelerators, which has the advantages of simple structure and high extraction efficiency. The optimum stripping point is a crucial factor influencing the quality and transmission efficiency of the extracted beam. An ensemble of particles to obtain the emittance, envelope and other parameters of the extracted beam. The precise location of the stripping foil is determined based on the real-space behavior of the tracking results in two adjacent turns, especially near the 11 MeV beam energy. The determination of the stripping point for the 11MeV extracted energy relies on two key criteria:

(1) The radial beam envelope is minimal in each turn, especially near the 11MeV energy range.

(2) When the condition outlined in (1) is met, the position of the beam emittance is minimum in each turn around the range of energy close to 11MeV.

The above two requirements can be used to successfully determine the appropriate stripping point. The exact position of the stripping foil is determined precisely by studying the azimuth and tilt angle of the stripping foil.

It is essential to achieve effective vertical focusing by selecting an azimuthal position of the stripping foil. The phase space distributions extracted at different azimuths of the stripping foil are shown in Fig.7(a)7(b). It is notable that while the axial distribution remains nearly elliptical due to the characteristics of multiple-turn extraction, the radial distribution of the bunch becomes non-elliptical as it traverses the stripping foil. This property contributes to an increase in the energy spread of the extracted beam. The azimuthal angle of 97^o is adopted to optimize beam focusing. It is a widely recognized that the angle between the stripping foil and the beam's normal direction can act as a focusing or defocusing lens in the radial direction, while having no impact on the axial direction. Fig.7(c)7(d) demonstrates the extracted beam envelope as a function of the rotation angle of the stripping foil. It is evident that this angle exerts a significant influence on the radial beam envelope, while its effect on the axial beam envelope is relatively minor. The tilt angle of 4^o is adopted to minimize the extracted beam envelope.

Stripping extraction has the advantages of high extraction efficiency and simple operation, but due to the existence of a large number of overlaps in the extraction region, it also brings great challenges to stripping extraction. Thus, a dual-opposite stripping foil device is utilized to improve the quality of the extracted beam. Fig.5(a) illustrates the basic principle of utilizing a dual-opposite stripper-extraction cyclotron to achieve extraction. The black line indicates the location of the stripper, which is installed in the valley. The beam is efficiently extracted utilizing two stripping foils positioned with an azimuthal difference of 175.26^o. The simulation results show that 96% of the macro-particles are successfully extracted by the first stripping foil. The remaining

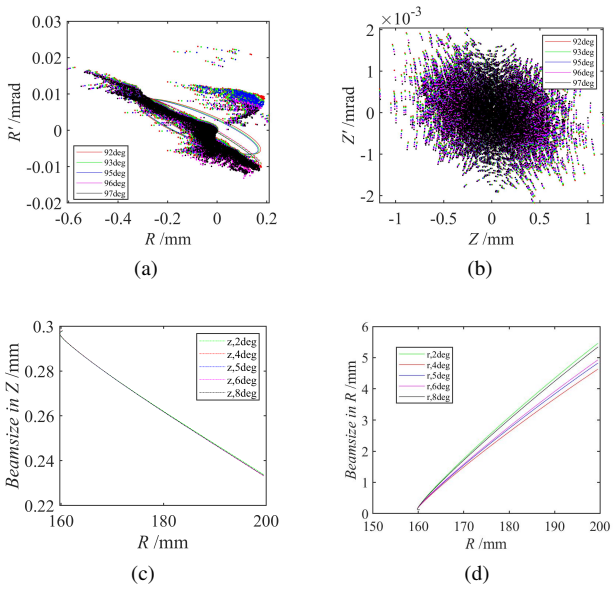

Fig. 7. (a)(b) the phase space distributions in radial and vertical as function of the azimuth of stripping foil; (c)(d) extraction beam envelope as function of rotation angle of stripping foil.

4% macro-particles are stripped and extracted by a second stripping foil. The beam size at the stripping foil measures $0.5\,\mathrm{mm} \times 3.4\,\mathrm{mm}$. It is worth noting that the radial emittance experiences a modest increase from $0.5\pi\ \mathrm{mm\,mrad}$ to $1.1\pi\ \mathrm{mm\,mrad}$, while the axial emittance exhibits a negligible change, is about $0.3\pi\ \mathrm{mm\,mrad}$. The energy spread with the beam at extraction is 0.0098 MeV.

VI. CONCLUSION

This paper presents a new design of a compact superconducting cyclotron for medical isotope production, with 11MeV energy and a 50μA beam current for H^- ions. Compared to the ION-12SC, it offers higher extracted beam intensity, which enhances production efficiency and makes it more suitable for producing PET isotopes. The study covers magnet system design, central region configuration, beam dynamics analysis, and extraction system design. The initial size of the magnet system is established according to the principles of magnetic circuit theory. Due to the complexity of magnet system design, precise beam dynamics simulations are carried out to fine tune the dimension of the magnetic sectors. After multiple iterations, the final magnet dimensions stand at 200mm in diameter and 730mm in height. The deviation of the obtained field from the isochronous field remains well within 10GS, and the orbital frequency error is on the of order 10^{-4}. Importantly, the beam dynamics calculations show that the tune does not intersect any hazardous resonance lines during acceleration.

The RF system employs the single 197^o Dee model to supply the axial focusing for beam in the first few turns. After optimization, the PIG ion source is positioned at (-0.2 mm, -7

mm). Assuming the ion source output slit energy of 20 eV and an initial beam emittances of 1.3π mm mrad, the transmission efficiency of the central region is enhanced from 26.5% to 40% through iterative modifications of the central electrode structure. The results reveal that after 191 turns of acceleration, the particle's energy reaches 11 MeV at the radius of 155 mm. Importantly, the RF phase extrusion remain within 5^o throughout the process. In addition, this paper studies the impact of beam emittance variation on the emittance of the extracted beam and the initial distribution of beam on the beam emittance during the acceleration process. It is worth noting that selecting the initial particles distribution in the radial stable region can effectively reduce the emittance growth during acceleration. As a result, the extracted beam emittance decreases from 3.92π mm mrad to 2.36π mm mrad. Furthermore, the oscillation range of the radial beam envelope exhibited a significant improvement, decreasing from 0.1 mm to 1.2 mm down to a much narrower range of 0.08 mm to 0.26 mm.

Stripping extraction is adopted due to the high efficiency of stripping extraction and the fact that its beam quality can meet the requirements of a cyclotron for radioisotope production. The stripping point at 11 MeV is calculated using the methodology of finding minimum beam size at the stripping foil, utilizing phase space distribution obtained from the multi-particle simulation, and conducting a detailed simulation of the extraction trajectory for the 11 MeV energy beam. The impact of the azimuthal position of the stripping foil and the tilt angle between the stripping foil and the beam on the quality of the extracted beam is studied. The azimuthal position of the stripping foil at 97^o and the tilt angle of 4^o is adopted. Notably, the energy spread is 0.0098 MeV for 11.12 MeV energy.

[1] X. H. wang, V. Smirnov, S. Vorozhtsov, Superconducting cyclotron for flash therapy. Nucl. Instrum. Nucl. Instrum. Methods Phys. Res. Sect. A **986**, 164742 (2021). DOI: 10.1016/j.nima.2020.164742

[2] R. Woo, M. song, D. Cho,*et al*., Feasibility study on the DFP adoption of the medical cyclotron decommissioning in Republic of Korea. Nucl. Sci. Tech. **25**, S1 (2014). DOI: 10.13538/j.1001-8042/nst.25.S010301

[3] T. J. zhang, Y. L. Lu, Z. G. Yin, *et al*., Overall design of CYCIAE-14, a 14 MeV PET cyclotron. Nucl. Instrum. Methods Phys. Res. Sect. B **269**, 24 (2011). DOI: 10.1016/j.nimb.2011.04.049

[4] T. J. zhang, S. Z. An, C. wang, *et al*., Physics design of a 70 MeV high intensity cyclotron, CYCIAE-70. Nucl. Instrum. Methods Phys. Res. Sect. B **269**, 24 (2011). DOI: 10.1016/j.nimb.2011.04.052

[5] M. Campbell, A. Tikka, Low-cost target system for neutron activation using a medical cyclotron. Application to the non-destructive analysis of gold and silver. Appl. Radiat. Isot. **184**, 110117 (2022). DOI: 10.1016/j.apradiso.2022.110117

[6] Y. C. Feng, M. Li, R. S. Mao, *et al*., Transverse emittance measurement for the heavy ion medical machine cyclotron. Nucl. Sci. Tech. **30**, 184 (2019). DOI: 10.1007/s41365-019-0699-7

[7] G. Dellepiane, P. Casolaro, C. Favaretto, *et al*., Cross-section measurement of thulium radioisotopes with an 18 MeV medical PET cyclotron for an optimized 165Er production. Appl. Radiat. Isot. **200**, 110954 (2023). DOI: 10.1016/j.apradiso.2023.110954

[8] G. Dellepiane, P. Casolaro, I. Mateu, *et al*., Alternative routes for 64cu production using an 18 MeV medical cyclotron in view of theranostic applications. Appl. Radiat. Isot. **191**, 110518 (2023). DOI: 10.1016/j.apradiso.2022.110518

[9] B. Qin, X. Liu, Q. S. chen, *et al*., Design and development of the beamline for a proton therapy system. Nucl. Sci. Tech. **32**, 138 (2021). doi: 10.1007/s41365-021-00975-y

[10] M. Li, J. X. zheng, Y. T. Song, *et al*., Beam optics and isocenter property of SC200 proton therapy gantry. Nucl. Sci. Tech. **29**: 112 (2018). DOI: 10.1007/s41365-018-0446-5

[11] T. J. zhang, C. wang, M. Li, *et al*., Developments for 230 MeV superconducting cyclotrons for proton therapy and proton irradiation. Nucl. Instrum. Methods Phys. Res. Sect. B **406**: 224–249 (2017). DOI: 10.1016/j.nimb.2016.11.010

[12] L. García-Tabarés, P. Abramian, C. Jesús, *et al*., Development of a superconducting magnet for a compact cyclotron for radioisotope production. IEEE Trans. Appl. Supercond. **26**: 1–4 (2016). DOI: 10.1109/TASC.2016.2548429

[13] P. Schmor, Review of cyclotrons for the production of radioactive isotopes for medical and industrial applications. Rev. Accel. Sci. Technol. **4**, 103–116 (2011). DOI: 10.1142/S1793626811000574

[14] DL. Friesel, TA. Antaya, Medical cyclotrons. Rev. Accel. Sci. Technol. **2**, 133–156 (2009). DOI: 10.1142/S1793626809000272

[15] J. S. Zhang, J. X. Zheng, Y. T. Song, *et al*., Design and field measurement of a dipole magnet for a newly developed superconducting proton cyclotron beamline. Nucl. Sci. Tech. **29**: 133 (2018). DOI: 10.1007/s41365-018-0463-4

[16] J. D. Long, Z. Yang, P. Dong, *et al*., Study on a cold-cathode H^- PIG-type ion source. Nucl. Sci. Tech. **24**: 040201 (2013). DOI: 10.13538/j.1001-8042/nst.2013.04.008

[17] S. Korenev, R. Dishman, A. Yebra, *et al*., Characterization of graphene stripper foils in 11-MeV cyclotrons. Phys. Procedia **90**, 369–373 (2017). DOI: 10.1016/j.phpro.2017.09.034

[18] https://www.3ds.com/products/simulia/opera

[19] X. H. wang, K. Z. Ding, Y. T. Song *et al*., Physical design of the beam injection system of a superconducting cyclotron using DONS code. Nucl. IEEE Trans. Appl. Supercond. **31**, 8 (2021). DOI: 10.1109/TASC.2021.3107823

[20] https://amas.web.psi.ch/opal/Documentation/2022.1/

[21] V. smirnov, Computer codes for beam dynamics analysis of cyclotronlike accelerators. Phys. Rev. Accel. Beams **20**, 124801 (2017). DOI: 10.1103/PhysRevAccelBeams.20.124801

[22] A.S. Zhong, G.F. Ping, X.H. Dong *et al*., Stripping extraction calculation and simulation for CYCIAE-100. Chin. Phys. C **33**, 42 (2009). DOI: 0.1088/1674-1137/33/S2/011

[23] L. H. Thomas, The paths of ions in the cyclotron I. orbits in the magnetic field. Phys. Rev. **54**, 580 (1938). DOI: 10.1103/PhysRev.54.580

[24] T. J. Zhang, C. Wang, T. Cui, *et al*., Design and Construction of the Main Magnet for a 230-MeV Superconducting Cyclotron. IEEE Trans. Appl. Supercond. **28**, 3 (2018). DOI: 10.1109/TASC.2017.2777469

[25] T. J. Zhang, L. Z. Guo, J. Q. Zhong, *et al*., Physics design of CYCAIE-100. Chin. Phys. C **33**, 33 (2009). DOI: 10.1088/1674-1137/33/S2/009

[26] M. M. Gordon, *Particle Accelerators*, 1nd edn. (Science Publishers, the United States of America, 1983), pp. 67–84 (1983)

[27] V. L. Smirnov, S. B. Vorozhtsov, J. Vincent, H^- superconducting cyclotron for PET isotope production. Phys. Part. Nucl. Lett. **11**, 774–787 (2014). DOI: 10.1134/S1547477114060132

[28] S. Du, C. Zou, K. Ding, *et al*., Design and test of superconducting magnet for 200 MeV proton cyclotron. Cryogenics **97**, 122–125 (2019). DOI: 10.1016/j.cryogenics.2018.11.004

[29] B. Qin, D. Z. chen, L. C. zhao, *et al*., An improved matrix method for magnet shimming in compact cyclotrons. Nucl. Instrum. Methods Phys. Res. Sect. A **620**, 121–127 (2010). DOI: 10.1016/j.nima.2010.03.135

[30] V. L. Smirnov, Central region design in a compact cyclotron. Phys. Part. Nucl. Lett. **16**, 34–45 (2019). DOI: 10.1134/S1547477119010114

[31] V. Smirnov, S. Vorozhtsov, J. Vincent, Design study of an ultra-compact superconducting cyclotron for isotope production. Nucl. Instrum. Methods Phys. Res., Sect. A. **763**, 6–12 (2014). DOI: 10.1016/j.nima.2014.06.013

[32] W. D. kilpatrick, criterion for vacuum sparking designed to include both rf and dc. Rev. Sci. Instrum. **28**, 10 (1957). DOI: 10.1063/1.1715731

[33] Y. D. Li, H. G. Wang, C. L. Liu, *et al*., Two-dimensional Child–Langmuir law of planar diode with finite-radius emitter. Appl. Surf. Sci. **251**, 1-4 (2005). DOI: 10.1016/j.apsusc.2005.03.160

[34] T. J. Zhang, H. J. Yao, F. P. Guan, *et al*., Spiral inflector and central region study for three cyclotrons at CIAE. Nucl. Instrum. Methods Phys. Res. Sect. B **261**, 1-2 (2007). DOI: 10.1016/j.nimb.2007.04.230

[35] A. M. Kolano, Dissertation(The university of Huddersfield, 2017)

[36] T. J. Zhang, M. Li, J. Q. Zhong, *et al*., Beam dynamics study for a small, high current 14 MeV PET cyclotron. Nucl. Instrum. Methods Phys. Res. Sect. B **269**, 24 (2011). DOI: 10.1016/j.nimb.2011.04.050